ACS Photonics

Article

pubs.acs.org/journal/apchd5

Influence of the Evanescent Field Decay Length on the Sensitivity of Plasmonic Nanodisks and Nanoholes

Francesco Mazzotta,[†] Timothy W. Johnson,[‡] Andreas B. Dahlin,[†] Jonah Shaver,[‡] Sang-Hyun Oh,*[,‡] and Fredrik Höök*[,†]

[†]Department of Applied Physics, Chalmers University of Technology, SE-41296 Gothenburg, Sweden

[‡]Department of Electrical and Computer Engineering, University of Minnesota, Minneapolis, Minnesota 55455, United States

ABSTRACT: We evaluate and compare the sensitivity of gold nanodisks on silica substrates and nanoholes made in silica-supported gold films, two of the most common sensor structures used in plasmonic biosensing. An alumina overcoat was applied by atomic layer deposition (ALD) to precisely control the interfacial refractive index and determine the evanescent plasmonic field decay length. The results are in good agreement with analytical models and biomolecular binding experiments for the two substrates. We found that nanodisks outperform nanoholes for thin dielectric coatings (<∼20 nm), while the opposite holds true for thicker coatings (>∼20 nm). The optimum nanoplasmonic transducer element for a given biorecognition reaction can be chosen based on experimentally determined bulk sensitivities/noise levels and theoretically estimated evanescent field decay lengths.

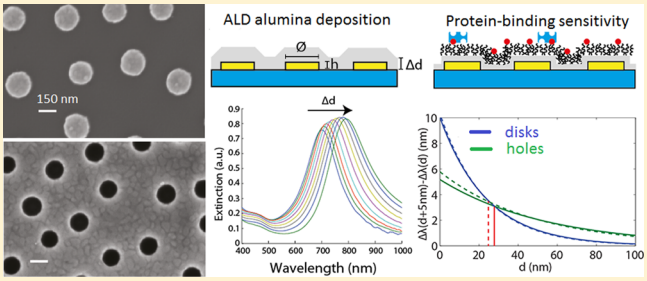

KEYWORDS: *plasmonics, biosensing, nanohole, nanodisk, surface plasmon resonance, atomic layer deposition*

Label-free surface-based bioanalytical sensors measure binding of target analytes to surface-immobilized molecular probes and are particularly useful in measuring the kinetics and affinity of biomolecular recognition reactions.[1,2] The use of nanoplasmonic sensors that harness the unique optical properties of metal nanostructures has greatly increased over the past several years. One common sensor format is based on the color change a nanoplasmonic substrate undergoes in response to changes in the interfacial refractive index. These changes can be induced by biomolecular binding within the structure's evanescent field, which is tightly confined to the metal−liquid interface.[3] The decay length of this evanescent field is typically on the order of tens of nanometers,[4−6] which matches the dimension of typical biomolecular components such as DNA, peptides, and proteins. As the refractive index changes associated with biomolecular binding reactions can be measured easily using ordinary optical spectroscopy, plasmonic nanostructures are in wide use for bioanalytical sensing.

While traditional evanescent-wave-based optical sensors such as conventional surface plasmon resonance (SPR)[7] or optical waveguides[8,9] have evanescent field decay lengths that extend up to hundreds of nanometers, nanoplasmonic sensors' evanescent fields only extend tens of nanometers into the solution. This disparity leads to higher sensitivity for bulk refractive index changes in conventional sensors than nanoplasmonic sensors, but similar signal-to-noise levels for detecting biomolecules.[10] This similarity in sensitivity is attributed to the significantly larger fraction of the evanescent field that is occupied by surface-bound biomolecules in the nanoplasmonic case. Furthermore, the tighter evanescent field localization in nanoplasmonic sensors renders them less susceptible to disturbing environmental effects such as changes in buffer composition and temperature.[11] These features, together with the simple instrumentation required to perform nanoplasmonic sensing, have motivated efforts to expand into demanding operational environments such as point-of-care medical diagnostics.[3] Significant efforts have also been invested to optimize biomolecular binding sensitivity by enhancing the local field strength with metal nanostructures of various shapes, such as rods and stars,[3,12] and spatial distributions.[13] In addition, designs that promote the generation of "hot spots", i.e., regions of high field strength, are also being pursued using closely aligned pairs of metal nanostructures.[14] More recently, focus has also been concentrated on monitoring information contained in the phase of the plasmonic resonance, which can potentially provide a higher figure of merit compared to simple intensity-based detection.[15,16]

In order to be detected, biorecognition events must occur within the shallow evanescent field, where the nanoplasmonic field strength is strongest. As the evanescent field has a spatial extension similar to the size of many biomolecules, this poses a seldom-addressed challenge in the context of practical bioanalytical sensor applications. This challenge stems from the fact that in order to prevent false positive signals due to nonspecific binding, the probe molecules should be immobilized on a layer designed to be inert to undesired biomolecular adsorption. Unfortunately, such layers often have thicknesses

Received: October 2, 2014
Published: December 16, 2014

DOI: 10.1021/ph500360d
ACS Photonics 2015, 2, 256−262

comparable to the extension of the evanescent field, forcing the biorecognition reaction to occur at a greater distance from the metal−liquid interface where the sensitivity is significantly reduced. Furthermore, as a rule of thumb, the thicker the coating, the more robust it becomes against nonspecific adsorption. For example, coatings made of short oligoethylene glycol (OEG) with a thickness of less than 5 nm can offer inertness toward diluted serum solutions,[17] but are outcompeted by >10 nm coatings made from high molecular weight polyethylene glycol (PEG) for complex biological fluids, lipid vesicle adsorption, and cellular attachment.[18,19]

Means to minimize the influence of inert coatings on the actual sensitivity of nanoplasmonic sensors have been analyzed and discussed by us and others in the case of single gold nanodisks,[20−22] pairs of gold nanodisks,[14,23] and gold films with nanoholes.[24−26] It has become clear from these studies that sensor designs with different decay lengths offer different sensitivities as a function of distance from the surface, but predicting which sensor design will provide the highest sensitivity for a given coating thickness remains a challenge. In order to select the nanoplasmonic sensor substrate best suited for a particular bioanalytical sensing application, the dependence of the absolute sensitivity on the distance from the sensor surface must be known. Without this information, one cannot optimize the sensor for the inert coating thickness required to offer sufficiently low nonspecific binding.

Atomic layer deposition (ALD) of alumina (Al_2O_3)[27] offers a precise means to experimentally determine the sensitivity reduction versus surface separation for nanoplasmonic sensors than layer-by-layer deposition of organic films on optical sensors.[6,28] We demonstrate this for two commonly used sensor substrates: short-range ordered gold nanodisks on silica substrates[16,21,22,29] and nanoholes made in optically thin gold films.[30−32] These structures were designed to be each other's inverse, with the spatial distribution (~15% surface coverage), diameter (110 and 150 nm), and height (20 and 30 nm) of the disks identical to the nanohole depths. Alumina ALD was used, as it offers high-quality film formation in terms of low pinhole density, homogeneous film thickness and density, and conformal step coverage, i.e., low influence from shadowing effects induced by the underlying nanostructure.[33−35] By depositing alumina films over the full extension of the evanescent field (up to ~90 nm) in 10 steps, both the absolute bulk sensitivity and the reduction in sensitivity were determined. The experimental results were also compared with estimates by analytical models representing changes in optical extinction and resonance shift upon coating of nanoplasmonic disks[36] and nanoholes[36−38] with a dielectric medium. The excellent agreement of the theoretically estimated decay lengths with experiment led us to combine this information with the easily measured bulk refractive index sensitivity, to predict the optimal sensor substrate for a given application. These predictions were successfully evaluated by recording specific binding of NeutrAvidin to biotin-containing PLL-*g*-PEG on alumina films of various thicknesses.

RESULTS AND DISCUSSION

Figure 1a shows representative scanning electron microscope (SEM) images of nanodisks and nanoholes with common diameters of 150 ± 10 nm and heights/depths, determined by the 30 nm evaporated gold film (schematic in Figure 1b). Figure 1c shows changes in optical extinction spectra in the visible to infrared (IR) region upon alumina ALD from 6 nm to between 40 and 90 nm in up to 10 steps.

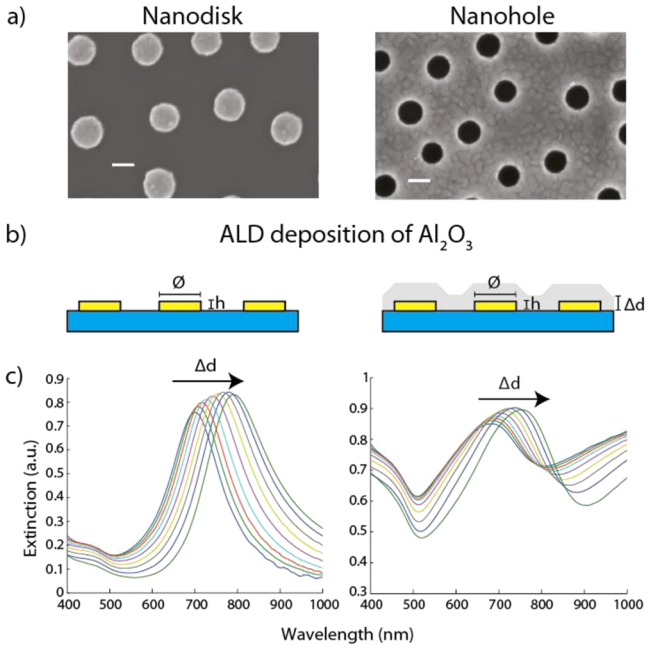

Figure 1. (a) SEM images of the plasmonic chips showing the characteristic spacing between disks/holes. The scale bar is 150 nm. (b) Schematic representation of the plasmonic structures upon ALD deposition of alumina. (c) Extinction spectra in air of two structures with a diameter/height ratio of 150:30 nm: nanodisks (left) and nanoholes (right).

The extinction peak position shifts toward longer wavelengths continually with increasing ALD film thickness. Its magnitude increases until 70 nm and then decreases, an effect attributed to optical interference within the dielectric coating. The decay length of the evanescent field and the sensitivity of the sensor substrates were evaluated using extinction spectra peak shifts upon alumina deposition. To determine the influence of the surrounding media on the decay length and sensitivity, peak-position shifts at each ALD step were measured in air (Figure 2a,b) and water (Figure 2c,d). In total, nanodisks and holes with diameter-to-height/depth ratios of 110:20 (Figure 2a,c) and 150:30 (Figure 2b,d) were analyzed in air and water, for a total of eight cases.

The absolute peak position shift upon initial alumina deposition (up to a thickness of around 10−20 nm) was significantly more pronounced (a factor of ~2) in air (Figure 2a,b) than in water (Figure 2c,d). This effect is attributed to the larger difference in refractive index between alumina and air than alumina and water. Upon further increase of the alumina film thickness, the peak shift saturates at between 70 and 90 nm for all substrates. Figure 2 shows that the overall sensitivity in both air and water is determined by the aspect ratio of the nanoscale features, while the decay length depends on the type of structure.

The dependence of the peak position shift on film thickness, d, can be expressed as[39,40]

$$\Delta\lambda = \frac{m}{\delta}\int_0^\infty \Delta n(z)\,\exp(-z/\delta)\,\mathrm{d}z \qquad (1)$$

where m corresponds to the bulk refractive index sensitivity ($\Delta\lambda$ at $d \to \infty$), Δn is the difference in refractive index between the adsorbed layer and the surrounding medium, and δ is the

DOI: 10.1021/ph500360d
ACS Photonics 2015, 2, 256−262

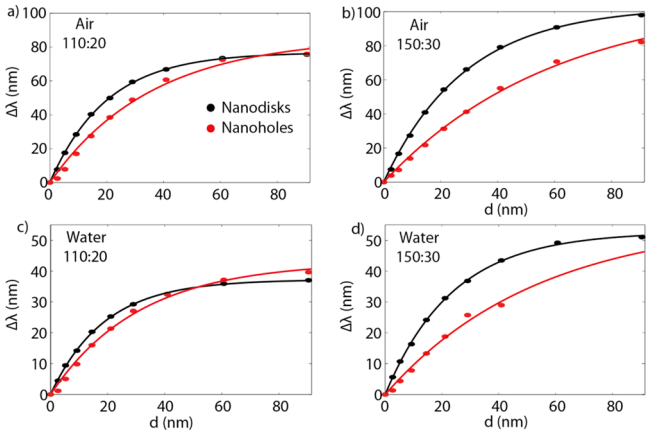

Figure 2. Plasmonic extinction peak position shift plotted versus alumina layer thickness. Samples with a diameter-to-height/depth of 110:20 (a and c) and 150:30 (b and d) were analyzed in air (a and b) and water (c and d). The experimental data were fit to a single-exponential function ($R^2 > 0.98$ for each fit). The sample-to-sample variation of the relative peak position shift was less than ±1 nm.

decay length of the evanescent field. For a homogeneous coating with thickness d deposited directly onto the surface, eq 1 was rewritten as

$$\Delta\lambda = m\Delta n[1 - \exp(-d/\delta)] \quad (2)$$

and used to determine m and δ for a fit to the experimental data (Figure 2). Using a refractive index of 1.65 for the ALD alumina overlayer[41] yields bulk sensitivity values, m, of 118 and 132 nm/refractive index unit (RIU) for 110:20 aspect ratio nanodisks and nanoholes, respectively, and 158 and 166 nm/RIU for the 150:30 samples. The m values obtained from the peak position shift upon immersing the uncoated substrates in water were within 10% of those obtained by ALD, verifying the refractive index value used for alumina is applicable.

We compared the results with theoretical predictions derived from analytical models (see Materials and Methods). Figure 3 shows the representative decay lengths obtained from the analysis of nanodisk and nanohole substrates with aspect ratios of 110:20 (Figure 3a) and 150:30 (Figure 3b), together with the decay lengths obtained from the theoretical representations.

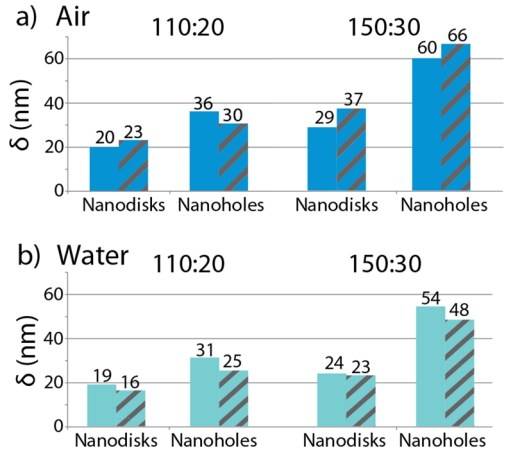

Figure 3. Decay length of the sensitivity is presented for the two structures (nanodisks and nanoholes) in air (a) and in water (b). The filled and striped bars represent the experimental values and theoretical predictions, respectively.

As shown in Figure 3, the decay length for nanodisks is roughly half that of nanoholes. The decay lengths for the 150:30 aspect ratio samples are nearly twice as long as the 110:20 samples. Furthermore, the theoretical predictions of the decay lengths match the experimental data for both structures in both media to within 4% in the best case and 25% in the worst. This level of agreement is within expected values considering the complexity of the substrates. The discrepancy between experiments and theory was more pronounced for the bulk sensitivity, however. In the case of nanodisks, the predicted bulk sensitivity was approximately 3 times larger than the experimental value, which can be attributed to the lack of accounting for the substrate in the model. For nanoholes, the predicted bulk sensitivity was approximately 30% smaller that the experimental value because the model does not include the dielectric coating inside the nanoholes. From this we conclude that the bulk sensitivity can be more readily obtained experimentally for these substrates, while the decay length can be determined using the proposed analytical models.

From Figure 3 one may intuitively believe that the longer decay length of the 150:30 nanohole substrates makes these sensor substrates the obvious choice in biorecognition situations requiring a thick, inert coating. However, for full consideration, one must also take the absolute peak-position shift into account. To evaluate this aspect, we plotted the peak shift induced by adding an additional 5 nm alumina film, in water, to each existing film thickness. Figure 4 uses data from

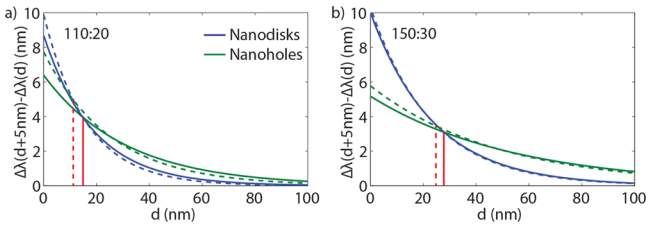

Figure 4. Estimated peak-position shift ($\Delta\lambda(d + \Delta d) - \Delta\lambda(d)$) for the adsorption of an additional 5 nm (Δd) thick alumina layer onto an existing alumina layer of thickness d in water. The solid lines represent the experimental data and the dashed lines the theoretical predictions. The red line marks the transition thickness of alumina at which nanodisks become less sensitive than nanoholes.

Figure 2 and the functional form $\Delta\lambda(d + \Delta d) - \Delta\lambda(d)$, with $\Delta d = 5$ nm. Theoretical predictions obtained from the estimated decay lengths using the analytical models are also shown.

Figure 4 shows a clear crossover point in peak shift performance between the nanoholes and nanodisks at a distance of 17 and 28 nm from the surface for 110:20 and 150:30 aspect ratios, respectively. This result suggests that for ~10 nm PEG coatings, demonstrated to render gold inert even in very complex environments,[42] modified with ~10 nm IgG antibodies 150:30 aspect-ratio nanodisks will show the highest sensitivity. If the antibodies and PEG layer are biotinylated and coupled using an intermediate avidin linker, however, the total film thickness will approach a regime where the nanohole substrate will produce the highest response. Similarly, nanoplasmonic detection of larger objects, in the tens to hundreds of nanometer range, such as viruses, lipid vesicles, or nanoholes, is likely to show better sensitivity than nanodisk substrates. These situations are analogous to the case of indirect sensing, where the sensor is coated with a dielectric film before the binding

DOI: 10.1021/ph500360d
ACS Photonics 2015, 2, 256−262

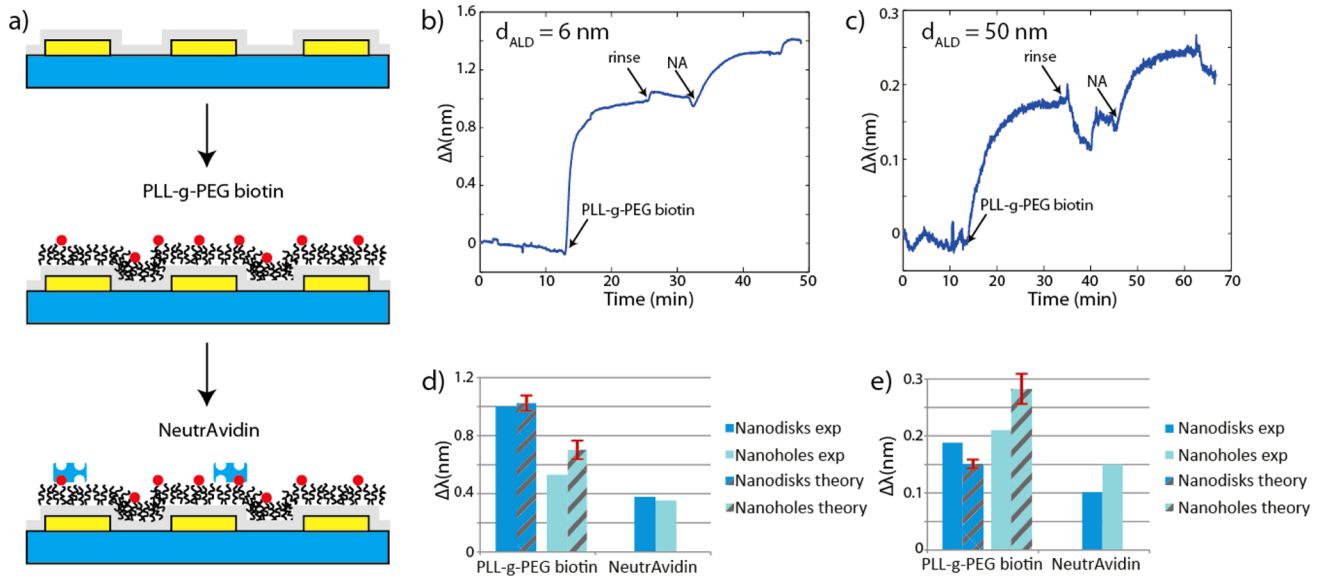

Figure 5. (a) Schematic representation of a biosensing experiment, adsorption of the probe molecules (biotinylated PLL-*g*-PEG), and binding of the target molecule (NeutrAvidin). (b) Peak shift versus time upon adsorption of PLL-*g*-PEG and NeutrAvidin on a (b) 6 nm and (c) 50 nm thick alumina coating on 150:30 aspect ratio nanoholes. The magnitude of the measured peak shifts at saturation for (d) a 6 nm thick alumina coating and (e) a 50 nm thick alumina coating of 150:30 aspect ratio nanoholes and nanodisks. The error bars represent the uncertainty of the theoretical prediction originating from uncertainties in reference values for mass uptake and thickness of the PLL-*g*-PEG layer.

experiment. In this case we are effectively increasing the distance from the sensor surface, allowing for further tuning and tailoring of the sensor response. This was demonstrated for supported lipid bilayer formation on silica-coated nanohole substrates[43] and for sintering of platinum nanoparticles.[44]

There is a broad range of sensing configurations, and the inherent possibility to optimize the design of nanoplasmonic sensors for predefined sensing situations is very attractive. It would be valuable to generate sensitivity-versus-thickness curves, e.g., Figure 4, without multiple rounds of time-consuming ALD. The good agreement between the theoretically predicted and experimentally determined decay lengths, straightforward bulk sensitivity determinations, and eq 2 enables just that. Using this combination we can generate sensitivity curves with a crossover point accuracy, i.e., the precise thickness at which one sensor type begins to outperform the other, better than 5 nm.

To evaluate the accuracy of this prediction in a real biomolecular sensing experiment, we monitored biotin-modified PLL-*g*-PEG adsorption followed by NeutrAvidin binding.[23] For this demonstration, we used 6 and 50 nm thick alumina coatings on 150:30 aspect ratio nanodisk and nanohole substrates (see schematic illustration in Figure 5a and raw data for nanoholes in Figure 5b and c).

Figure 5b and c show changes in peak position versus time for two identical nanodisk substrates with alumina coatings of 6 and 50 nm. The reduction in absolute response is around a factor of 5, in good agreement with the predicted value in Figure 4. A summary of the two-step adsorption process for 150:30 aspect ratio nanodisk and nanohole substrates with 6 and 50 nm alumina coatings is shown in Figure 5d and e. The nanodisk substrate outperforms the nanohole substrate by a factor of ∼2 for PLL-*g*-PEG adsorption in the case of the thinner (6 nm) alumina coating, while the opposite holds for the thicker (50 nm) alumina coating, in agreement with the predictions. The differences are less dramatic for NeutrAvidin binding, which we attribute to its tendency to penetrate into the PLL-*g*-PEG film.

The agreement with the theoretical predictions raised the possibility of using measured bulk sensitivities and the theoretically determined decay lengths to predict the expected experimental response due to PLL-*g*-PEG adsorption. To do so, both the change in effective refractive index, Δn, and the PLL-*g*-PEG film thickness, d, must be known. Previous mass-uptake determinations of PLL-*g*-PEG to oxides ranged between 123 ± 4 and 148 ± 10 ng/cm^2,[45] producing film thicknesses of around 11 ± 4 nm.[46] Using de Feijter's formalism[47] these numbers for the adsorbed mass, Γ, can be related to Δn in eq 2 by

$$\Delta n = \frac{\Gamma \mathrm{d}n/\mathrm{d}c}{d} \tag{3}$$

A refractive index increment,[48] $\mathrm{d}n/\mathrm{d}c = 0.169$ g/cm^3, for PLL-*g*-PEG gives Δn ranging from 0.02 to 0.025. As seen in Figure 5d and e, the theoretical predictions of the expected peak shift upon PLL-*g*-PEG binding are within 25% for both the 6 and 50 nm alumina coating.

In conclusion, we have demonstrated a straightforward means to select the nanodisk or nanohole geometry best suited for a given biorecognition reaction by combining theoretically calculated evanescent field decay lengths with experimentally measured nanoplasmonic substrate sensitivities. It should be noted that the plasmonic field extension estimates, both by theory and experiment, are providing the effective decay length in a medium with a refractive index equal to that of the coating material. The decay length in the actual medium in which the sensing experiments are performed will be slightly different (longer for less optically dense materials). For instance, a surface plasmon in water typically has its field decay reduced by 10−20% compared to air.[49] For higher accuracy one should ideally coat with a material that has a refractive index just slightly different from water or employ more detailed iterative models.[50] One parameter that must also be considered, but is beyond the scope of this work, is the instrumental resolution.

DOI: 10.1021/ph500360d
ACS Photonics 2015, 2, 256−262

The minimum peak position change that can be detected may vary for different nanoplasmonic sensor and instrument designs. For the substrates and instrumentation used here, the resolution was close to 5×10^{-3} nm; however it can vary quite dramatically depending on the shape of the extinction spectra and details of the optical setup used.[30] Extending this work from bioanalytical sensing on dielectric-coated nanoplasmonic substrates[43] to other branches of nanoplasmonic sensing, e.g., indirect sensing in catalysis applications,[51] could be quite promising. Our technique could, for example, be applied to nanocatalyst investigations where support material thickness could be tailored to optimize transducer element sensitivity with the chemical stability and support morphology.

MATERIALS AND METHODS

Substrate Fabrication. The sensor chips were fabricated on 0.1 mm thick glass substrates (Gerhard Menzel GmbH, Germany). Gold films with nanoholes were deposited by means of colloidal lithography.[52] In brief, polystyrene colloids of the desired size (110 or 150 nm) were first adsorbed onto a glass substrate. The colloids self-arrange into a short-range ordered pattern, with a nearest neighbor distance determined by interparticle electrostatic repulsion.[52] A gold film of the desired thickness (20 or 30 nm, with a 1 nm thick chromium adhesion layer) was then deposited onto the substrate by electron beam assisted evaporation (PVD225, Kurt J. Lesker Company, UK). Last, the colloidal particles were removed from the substrate with adhesive tape, exposing the nanoholes. The gold nanodisks were fabricated using hole-mask colloidal lithography.[53] In brief, a 120 nm sacrificial layer of poly(methyl methacrylate) (PMMA) was spin coated onto the substrate. The colloids were then adsorbed onto the PMMA layer from an aqueous solution. A 15 nm chromium film was evaporated to serve as a metal mask for the fabrication of discrete gold nanodisks. The mask was patterned by removal of the colloids by tape stripping. The pattern was then transferred onto the PMMA layer by oxygen plasma (BatchTop m/95, Plasmatherm, USA), allowing for gold deposition directly onto the substrate. A gold film was evaporated, forming the nanodisks, and the remaining material was removed by PMMA lift-off.

Atomic Layer Deposition. In this study ALD was used to create conformal layers of alumina on the sensor substrates.[54,55] The alumina ALD process makes use of two precursors, trimethylaluminum and H_2O, which are alternately pulsed and purged through a vacuum chamber.[27] Each precursor initiates a self-limiting reaction on the sensor surface, one cycle forming a single monolayer, allowing angstrom-level film deposition resolution. The deposition was done at 250 °C, and the thickness measured via ellipsometry (Rudolph, MS14C2C) on a silicon reference wafer after each step.

Optical Characterization of the Plasmonic Substrates. Extinction spectra of the sensor substrates were obtained by transmission spectroscopy. The samples were illuminated with a white light source (quartz tungsten-halogen lamp, Newport, USA), and the transmitted light was collected through an optical fiber directed to a spectrometer with a back-thinned CCD (QE65000, OceanOptics, USA). The extinction spectra, $E(\lambda)$, were calculated according to

$$E(\lambda) = -\log_{10}\left(\frac{I_{\text{sample}}(\lambda) - I_{\text{dark}}(\lambda)}{I_{\text{ref}}(\lambda) - I_{\text{dark}}(\lambda)}\right)$$

where $I_{\text{sample}}(\lambda)$ is the spectrum of the sample, $I_{\text{dark}}(\lambda)$ a spectrum acquired without illumination, and $I_{\text{ref}}(\lambda)$ that of a reference substrate without nanoplasmonic structures. The centroid of the extinction spectrum was acquired in real time with a custom-designed LabVIEW program as described in ref 30.

Analytical Models. The resonance wavelength and the full extinction spectra of nanodisks were modeled using analytical theory as described previously.[36,37,56] Electrostatic theory was used to calculate the polarizability of an oblate (disk-like) spheroid. The modified long-wavelength approximation was used to account for the fact that the disks are relatively large, which introduces retardation effects and radiative damping. The cross section was acquired from the imaginary part of the polarizability and the incident wavevector. The permittivity of gold was described by an analytical model,[38] and all dielectric materials were treated as nonlossy and nondispersive. The limitation of this model is that the solid support was not taken into account, which results in an overestimation of the shift due to a high refractive index coating. However, the decay length can still be calculated with high accuracy even if the shift is overestimated. Introducing a glass support in the model is possible by a weighting factor corresponding to the area fraction in contact with the structure.[57,58] This did not result in a significant change in the decay length estimation (~7% difference for particles on a glass with $n = 1.52$), but only in the peak position shift.

To model the resonance shift of the nanoholes, we used a theoretical framework for surface waves in arbitrary thin-film multilayers.[36−38] The short-range ordered nanoholes enable grating-type coupling to bonding mode surface plasmons in the thin gold film; that is, short-range order is essentially equivalent to long-range order.[59] By calculating the dispersion relation of the surface plasmons for different refractive indices on the top of the metal film and assuming the wavevector remains the same for the surface plasmons at resonance (defined by the periodicity of the holes), a resonance peak shift can be predicted. The limitation of this model is that in reality the coating appears also inside the holes, while the model treats the structure as a one-dimensional thin-film system. This leads to an underestimation of the resonance shift since the RI is also increased inside the holes. However, just as with the model used to represent the nanodisk substrate, the decay length can still be calculated with high accuracy even if the shift is overestimated. The decay length is an intrinsic property of the calculated surface plasmon. Previous results indicate that although the near field is changed locally at the holes, the field extensions are similar to those calculated for thin films without holes.[59,60]

Functionalization of the Sensor Chip and Biosensing. The sensor chips were functionalized by adsorption of a solution containing a 0.1 mg/mL 4:1 (by weight) mixture of PEG grafted to poly L-lysine (PLL-*g*-PEG) and biotinylated PEG (PEGbiotin) (SuSoS AG, Switzerland) dissolved in phosphate-buffered saline (PBS) buffer (0.01 M phosphate buffer, 0.0027 M potassium chloride, 0.137 M sodium chloride, 7.4 pH). Afterward, the sensor chips were rinsed with PBS buffer followed by addition of a solution of 10 μg/mL NeutrAvidin dissolved in PBS buffer. The adsorption measurements were carried out under stagnant liquid conditions in a custom-made flow cell designed for transmission optical spectroscopy and complete exchange of the solution upon injection of 1 mL during 10 s.

DOI: 10.1021/ph500360d
ACS Photonics 2015, 2, 256−262

AUTHOR INFORMATION

Corresponding Authors

*E-mail: sang@umn.edu.

*E-mail: fredrik.hook@chalmers.se.

Notes

The authors declare no competing financial interest.

ACKNOWLEDGMENTS

The SSF-funded Functional Metamaterial Program and the Swedish Research Council are acknowledged for financial support. T.W.J. and S.-H.O. acknowledge support from the U.S. National Science Foundation (NSF CAREER Award).

REFERENCES

(1) Homola, J.; Yee, S. S.; Gauglitz, G. Surface plasmon resonance sensors: review. *Sens. Actuators, B* **1999**, *54*, 3−15.

(2) Nirschl, M.; Reuter, F.; Vörös, J. Review of transducer principles for label-free biomolecular interaction analysis. *Biosensors* **2011**, *1*, 70−92.

(3) Estevez, M.-C.; Otte, M. A.; Sepulveda, B.; Lechuga, L. M. Trends and challenges of refractometric nanoplasmonic biosensors: a review. *Anal. Chim. Acta* **2014**, *806*, 55−73.

(4) Kelly, K.; Coronado, E.; Zhao, L.; Schatz, G. C. The optical properties of metal nanoparticles: the influence of size, shape, and dielectric environment. *J. Phys. Chem. B* **2003**, *107*, 668−677.

(5) Rindzevicius, T.; Alaverdyan, Y.; Dahlin, A.; Höök, F.; Sutherland, D. S.; Käll, M. Plasmonic sensing characteristics of single nanometric holes. *Nano Lett.* **2005**, *5*, 2335−2339.

(6) Rindzevicius, T.; Alaverdyan, Y.; Kall, M.; Murray, W. A.; Barnes, W. L. Long-range refractive index sensing using plasmonic nanostructures. *J. Phys. Chem. C* **2007**, *111*, 11806−11810.

(7) Liedberg, B.; Nylander, C.; Lundström, I. Surface plasmon resonance for gas detection and biosensing. *Sens. Actuators* **1983**, *4*, 299−304.

(8) Michielin, O.; Ramsden, J. J.; Vergères, G. Unmyristoylated MARCKS-related protein (MRP) binds to supported planar phosphatidylcholine membranes. *Biochim. Biophys. Acta* **1998**, *1375*, 110−116.

(9) Székács, I.; Kaszás, N.; Gróf, P.; Erdélyi, K.; Szendrő, I.; Mihalik, B.; Pataki, A.; Antoni, F. A.; Madarász, E. Optical waveguide lightmode spectroscopic techniques for investigating membrane-bound ion channel activities. *PLoS One* **2013**, *8*, e81398.

(10) Svedendahl, M.; Chen, S.; Dmitriev, A.; Käll, M. Refractometric sensing using propagating versus localized surface plasmons: a direct comparison. *Nano Lett.* **2009**, *9*, 4428−4433.

(11) Anker, J. N.; Hall, W. P.; Lyandres, O.; Shah, N. C.; Zhao, J.; Van Duyne, R. P. Biosensing with plasmonic nanosensors. *Nat. Mater.* **2008**, *7*, 442−453.

(12) Dahlin, A. B.; Wittenberg, N. J.; Höök, F.; Oh, S.-H. Promises and challenges of nanoplasmonic devices for refractometric biosensing. *Nanophotonics* **2013**, *2*, 83−101.

(13) Hanarp, P.; Käll, M.; Sutherland, D. S. Optical properties of short range ordered arrays of nanometer gold disks prepared by colloidal lithography. *J. Phys. Chem. B* **2003**, *107*, 5768−5772.

(14) Aćimović, S. S.; Kreuzer, M. P.; González, M. U.; Quidant, R. Plasmon near-field coupling in metal dimers as a step toward single-molecule sensing. *ACS Nano* **2009**, *3*, 1231−1237.

(15) Kravets, V. G.; Schedin, F.; Jalil, R.; Britnell, L.; Gorbachev, R. V.; Ansell, D.; Thackray, B.; Novoselov, K. S.; Geim, A. K.; Kabashin, A. V.; Grigorenko, A. N. Singular phase nano-optics in plasmonic metamaterials for label-free single-molecule detection. *Nat. Mater.* **2013**, *12*, 304−309.

(16) Lodewijks, K.; Roy, W. V.; Borghs, G.; Lagae, L.; Van Dorpe, P. Boosting the figure-of-merit of LSPR-based refractive index sensing by phase-sensitive measurements. *Nano Lett.* **2012**, *12*, 1655−1659.

(17) Nilebäck, E.; Feuz, L.; Uddenberg, H.; Valiokas, R.; Svedhem, S. Characterization and application of a surface modification designed for QCM-D studies of biotinylated biomolecules. *Biosens. Bioelectron.* **2011**, *28*, 407−413.

(18) Andreasson-Ochsner, M.; Romano, G.; Hakanson, M.; Smith, M. L.; Leckband, D. E.; Textor, M.; Reimhult, E. Single cell 3-D platform to study ligand mobility in cell-cell contact. *Lab Chip* **2011**, *11*, 2876−2883.

(19) Gillich, T.; Benetti, E. M.; Rakhmatullina, E.; Konradi, R.; Li, W.; Zhang, A.; Schluter, A. D.; Textor, M. Self-assembly of focal point oligo-catechol ethylene glycol dendrons on titanium oxide surfaces: adsorption kinetics, surface characterization, and nonfouling properties. *J. Am. Chem. Soc.* **2011**, *133*, 10940−10950.

(20) Chen, S.; Svedendahl, M.; Käll, M.; Gunnarsson, L.; Dmitriev, A. Ultrahigh sensitivity made simple: nanoplasmonic label-free biosensing with an extremely low limit-of-detection for bacterial and cancer diagnostics. *Nanotechnology* **2009**, *20*, 434015.

(21) Otte, M.; Estévez, M.; Carrascosa, L.; González-Guerrero, A.; Lechuga, L. M.; Sepulveda, B. Improved biosensing capability with novel suspended nanodisks. *J. Phys. Chem. C* **2011**, *115*, 5344−5351.

(22) Mazzotta, F.; Wang, G.; Hägglund, C.; Höök, F.; Jonsson, M. P. Nanoplasmonic biosensing with on-chip electrical detection. *Biosens. Bioelectron.* **2010**, *26*, 1131−1136.

(23) Feuz, L.; Jonsson, M. P.; Höök, F. Material-selective surface chemistry for nanoplasmonic sensors: optimizing sensitivity and controlling binding to local hot spots. *Nano Lett.* **2012**, *12*, 873−879.

(24) Feuz, L.; Jönsson, P.; Jonsson, M. P.; Höök, F. Improving the limit of detection of nanoscale sensors by directed binding to high-sensitivity areas. *ACS Nano* **2010**, *4*, 2167−2177.

(25) Jonsson, M. P.; Dahlin, A. B.; Feuz, L.; Petronis, S.; Höök, F. Locally functionalized short-range ordered nanoplasmonic pores for bioanalytical sensing. *Anal. Chem.* **2010**, *82*, 2087−2094.

(26) Escobedo, C.; Chou, Y.-W.; Rahman, M.; Duan, X.; Gordon, R.; Sinton, D.; Brolo, A. G.; Ferreira, J. Quantification of ovarian cancer markers with integrated microfluidic concentration gradient and imaging nanohole surface plasmon resonance. *Analyst* **2013**, *138*, 1450−1458.

(27) Im, H.; Lindquist, N. C.; Lesuffleur, A.; Oh, S.-H. Atomic layer deposition of dielectric overlayers for enhancing the optical properties and chemical stability of plasmonic nanoholes. *ACS Nano* **2010**, *4*, 947−954.

(28) Luchansky, M. S.; Washburn, A. L.; Martin, T. A.; Iqbal, M.; Gunn, L. C.; Bailey, R. C. Characterization of the evanescent field profile and bound mass sensitivity of a label-free silicon photonic microring resonator biosensing platform. *Biosens. Bioelectron.* **2010**, *26*, 1283−1291.

(29) Larsson, E. M.; Millet, J.; Gustafsson, S.; Skoglundh, M.; Zhdanov, V. P.; Langhammer, C. Real time indirect nanoplasmonic in situ spectroscopy of catalyst nanoparticle sintering. *ACS Catal.* **2012**, *2*, 238−245.

(30) Dahlin, A.; Tegenfeldt, J.; Höök, F. Improving the instrumental resolution of sensors based on localized surface plasmon resonance. *Anal. Chem.* **2006**, *78*, 4416−4423.

(31) Gao, D.; Chen, W.; Mulchandani, A.; Schultz, J. S. Detection of tumor markers based on extinction spectra of visible light passing through gold nanoholes. *Appl. Phys. Lett.* **2007**, *90*, 073901.

(32) Zhang, X.; Hicks, E. M.; Zhao, J.; Schatz, G. C.; Van Duyne, R. P. Electrochemical tuning of silver nanoparticles fabricated by nanosphere lithography. *Nano Lett.* **2005**, *5*, 1503−1507.

(33) Elam, J.; Routkevitch, D.; Mardilovich, P.; George, S. Conformal coating on ultrahigh-aspect-ratio nanopores of anodic alumina by atomic layer deposition. *Chem. Mater.* **2003**, *15*, 3507−3517.

(34) Knez, M.; Nielsch, K.; Niinistö, L. Synthesis and surface engineering of complex nanostructures by atomic layer deposition. *Adv. Mater.* **2007**, *19*, 3425−3438.

(35) Lee, S. H.; Johnson, T. W.; Lindquist, N. C.; Im, H.; Norris, D. J.; Oh, S.-H. Linewidth-optimized extraordinary optical transmission in water with template-stripped metallic nanohole arrays. *Adv. Funct. Mater.* **2012**, *22*, 4439−4446.

DOI: 10.1021/ph500360d
ACS Photonics 2015, 2, 256−262

(36) Dahlin, A. B.; Zahn, R.; Vörös, J. Nanoplasmonic sensing of metal-halide complex formation and the electric double layer capacitor. *Nanoscale* **2012**, *4*, 2339−2351.
(37) Dahlin, A. B.; Sannomiya, T.; Zahn, R.; Sotiriou, G. A.; Vörös, J. Electrochemical crystallization of plasmonic nanostructures. *Nano Lett.* **2011**, *11*, 1337−1343.
(38) Ikenoya, Y.; Susa, M.; Shi, J.; Nakamura, Y.; Dahlin, A. B.; Sannomiya, T. Optical resonances in short-range ordered nanoholes in ultrathin aluminum/aluminum nitride multilayers. *J. Phys. Chem. C* **2013**, *117*, 6373−6382.
(39) Stewart, M. E.; Anderton, C. R.; Thompson, L. B.; Maria, J.; Gray, S. K.; Rogers, J. A.; Nuzzo, R. G. Nanostructured plasmonic sensors. *Chem. Rev.* **2008**, *108*, 494−521.
(40) Kedem, O.; Tesler, A.; Vaskevich, A.; Rubinstein, I. Sensitivity and optimization of localized surface plasmon resonance transducers. *ACS Nano* **2011**, *5*, 748−760.
(41) Yun, S. J.; Lee, K.-H.; Skarp, J.; Kim, H.-R.; Nam, K.-S. Dependence of atomic layer-deposited Al_2O_3 films characteristics on growth temperature and Al precursors of $Al(CH_3)_3$ and $AlCl_3$. *J. Vac. Sci. Technol., A* **1997**, *15*, 2993.
(42) Unsworth, L. D.; Sheardown, H.; Brash, J. L. Polyethylene oxide surfaces of variable chain density by chemisorption of PEO-thiol on gold: adsorption of proteins from plasma studied by radiolabelling and immunoblotting. *Biomaterials* **2005**, *26*, 5927−5933.
(43) Jonsson, M. P.; Jönsson, P.; Dahlin, A. B.; Höök, F. Supported lipid bilayer formation and lipid-membrane-mediated biorecognition reactions studied with a new nanoplasmonic sensor template. *Nano Lett.* **2007**, *7*, 3462−3468.
(44) Larsson, E.; Langhammer, C.; Zorić, I.; Kasemo, B. Nanoplasmonic probes of catalytic reactions. *Science* **2009**, *326*, 1091−1094.
(45) Huang, N.; Michel, R.; Voros, J.; Textor, M. Poly (L-lysine)-g-poly (ethylene glycol) layers on metal oxide surfaces: surface-analytical characterization and resistance to serum and fibrinogen adsorption. *Langmuir* **2001**, 489−498.
(46) Sannomiya, T.; Balmer, T. E.; Heuberger, M.; Vörös, J. Simultaneous refractive index and thickness measurement with the transmission interferometric adsorption sensor. *J. Phys. D: Appl. Phys.* **2010**, *43*, 405302.
(47) de Feijter, J. A.; Benjamins, J.; Veer, F. A. Ellipsometry as a tool to study the adsorption behavior of synthetic and biopolymers at the air-water interface. *Biopolymers* **1978**, *17*, 1759−1772.
(48) Lee, S.; Müller, M.; Ratoi-Salagean, M.; Vörös, J. Boundary lubrication of oxide surfaces by poly (L-lysine)-g-poly (ethylene glycol)(PLL-g-PEG) in aqueous media. *Tribol. Lett.* **2003**, *15*, 231−239.
(49) Jung, L. S.; Nelson, K. E.; Stayton, P. S.; Campbell, C. T. Binding and dissociation kinetics of wild-type and mutant streptavidins on mixed biotin-containing alkylthiolate monolayers. *Langmuir* **2000**, *16*, 9421−9432.
(50) Schoch, R. L.; Lim, R. Y. H. Non-Interacting Molecules as Innate Structural Probes in Surface Plasmon Resonance. *Langmuir* **2013**, *29*, 4068−4076.
(51) Larsson, E. M.; Langhammer, C.; Zoric, I.; Kasemo, B. Nanoplasmonic probes of catalytic reactions. *Science* **2009**, *326*, 1091−1094.
(52) Hanarp, P.; Sutherland, D. S.; Gold, J.; Kasemo, B. Control of nanoparticle film structure for colloidal lithography. *Colloids Surf., A* **2003**, *214*, 23−36.
(53) Fredriksson, H.; Alaverdyan, Y.; Dmitriev, a.; Langhammer, C.; Sutherland, D. S.; Zäch, M.; Kasemo, B. Hole−Mask Colloidal Lithography. *Adv. Mater.* **2007**, *19*, 4297−4302.
(54) Lindquist, N. C.; Nagpal, P.; McPeak, K. M.; Norris, D. J.; Oh, S.-H. Engineering metallic nanostructures for plasmonics and nanophotonics. *Rep. Prog. Phys.* **2012**, *75*, 036501.
(55) Whitney, A. V.; Elam, J. W.; Zou, S.; Zinovev, A. V.; Stair, P. C.; Schatz, G. C.; Van Duyne, R. P. Localized surface plasmon resonance nanosensor: a high-resolution distance-dependence study using atomic layer deposition. *J. Phys. Chem. B* **2005**, *109*, 20522−20528.
(56) Dahlin, A. B. *Plasmonic Biosensors: An Integrated View of Refractometric Detection*; Ios Press, 2012.
(57) Kelly, K.; Coronado, E.; Zhao, L.; Schatz, G. The optical properties of metal nanoparticles: the influence of size, shape, and dielectric environment. *J. Phys. Chem. B* **2003**, *107*, 668−677.
(58) Duval Malinsky, M.; Kelly, K. L.; Schatz, G. C.; Van Duyne, R. P. Nanosphere lithography: effect of substrate on the localized surface plasmon resonance spectrum of silver nanoparticles. *J. Phys. Chem. B* **2001**, *105*, 2343−2350.
(59) Sannomiya, T.; Scholder, O.; Jefimovs, K.; Hafner, C.; Dahlin, A. B. Investigation of plasmon resonances in metal films with nanohole arrays for biosensing applications. *Small* **2011**, *7*, 1653−1663.
(60) Junesch, J.; Sannomiya, T.; Dahlin, A. B. Optical properties of nanohole arrays in metal-dielectric double films prepared by mask-on-metal colloidal lithography. *ACS Nano* **2012**, *6*, 10405−10415.

DOI: 10.1021/ph500360d
ACS Photonics 2015, 2, 256−262